ARTICLE

Neuromedin U 'innervation' reprograms myeloid immunosuppression in neuroendocrine prostate cancer

Michela Perego[1,2✉], Jozef Madzo[3], Andrew V. Kossenkov[1,3], F. Cansu Atilgan[1,2], Marcella Tazzari[4], Maria Maddalena Tumedei[4], Francesco Limarzi[5], Cristian Lolli[6], Giorgia Gurioli[7], Alessandro Fatatis[8], Mary V. Iacocca[9,10], Nicholas J. Petrelli[9], Justine J. Jacobi[1,11], David W. Goodrich[1,11], Lucia R. Languino[1,12] and Dario C. Altieri[1,2]

© The Author(s), under exclusive licence to Springer Nature Limited 2026

Neuroendocrine prostate cancer (NEPC) is an increasingly recognized, highly aggressive disease variant with no actionable therapeutic targets and a life expectancy of 7 months or less. Using a transgenic mouse model, we now show that early stages of NEPC are associated with increased intraprostatic recruitment of Ly6G$^+$ polymorphonuclear neutrophils (PMN) and reduced infiltration of CD8$^+$ T cells. This coincided with expansive transcriptional changes of increased cell viability and cell migration, as well as upregulation of multiple neuronal mediators with the neuropeptide, Neuromedin U (NMU) as the top hit (Z score = 4.34; FDR < 5%; $p = 3.62 \times 10^{-9}$). Analysis of a large cohort of human patient samples revealed that NMU was highly expressed in early and late stage prostate cancer, preferentially segregating with AR$^-$/NE$^+$ metastases. Exposure of PMN to recombinant NMU was sufficient to stimulate cell migration, inflammatory gene expression with increased levels of the cytokine-like *alarmin*, S100A9 and suppression of T cell proliferation. Genetic or pharmacological targeting of NMU/S100A9 signaling inhibited NEPC growth, reinvigorated an intratumoral immune microenvironment via recruitment of tumor antigen-specific CD8$^+$ T cells with 'stem-like' (TCF1$^+$/PD1$^+$) and cytotoxic (GrzB$^+$/KLRG1$^+$) properties and enhanced the activity of therapeutic immune checkpoint inhibition, in vivo. Therefore, NMU 'innervation' drives myeloid immunosuppression in NEPC and provides a therapeutic target to restore sensitivity to immunotherapy in this highly refractory malignancy.

Oncogene (2026) 45:4442–4453; https://doi.org/10.1038/s41388-026-03969-5

INTRODUCTION

Tumor cells establish an expansive, bidirectional crosstalk with the nervous system [1], which is now recognized as a disease driver and potential therapeutic opportunity [2]. The cancer-neuronal axis is evident in prostate cancer [3], where a multidimensional process of "innervation" [4] promotes early- and late-stage mechanisms of tumor progression via adrenergic (sympathetic) and cholinergic (parasympathetic) signaling [5, 6]. This involves the release of multiple neurotrophins, such NGF that affect tumor cell proliferation, survival, and invasiveness [7], but also a comprehensive reprogramming of an immunosuppressive microenvironment [8], via recruitment of myeloid-derived suppressor cells (MDSC), CD8$^+$ T cell exhaustion, and upregulation of immune inhibitory receptors [9, 10].

Such tumor "innervation" plays a critical role in neuroendocrine prostate cancer (NEPC) [11]. Long considered as a rare and unrepresentative disease variant, we now know that NEPC is instead an urgent and expanding problem [12, 13], developing in up to 25% of prostate cancer patients receiving treatment with androgen-deprivation therapy (ADT) and androgen receptor (AR) signaling inhibitors (ARSi) [14]. Characterized by neuronal de-differentiation [15], expression of neuroendocrine markers [16, 17], loss of luminal epithelial traits [18] and lack of androgen receptor (AR) signaling [19], NEPC rapidly metastasizes to bone and visceral organs, establishes a profoundly immunosuppressive microenvironment, and is highly treatment-resistant, carrying a life expectancy of only 7 months or less [20].

Despite the clear role in disease progression [21], strategies to target the cancer-neuronal axis, let alone in NEPC [22], are still in infancy [23], and the goal of disabling a "neuronal" immunosuppressive microenvironment [24] to restore sensitivity to immune checkpoint inhibition remains to be realized [25]. In this context, a candidate regulator at the interface between neuronal signaling and immune-inflammatory responses [26–28] Neuromedin U (NMU) [29]. An evolutionary conserved polypeptide of 25 amino acids in humans, NMU orchestrates a broad signaling network [30] that controls smooth muscle cell contraction, metabolic homeostasis, blood pressure changes, stress response, and hormone

[1]Prostate Cancer Discovery and Development Group, Philadelphia, PA, USA. [2]Gene Regulation and Cell Signaling Program, The Wistar Institute, Philadelphia, PA, USA. [3]Bioinformatics Shared Resource, The Wistar Institute, Philadelphia, PA, USA. [4]Advanced Cellular Therapies and Rare Tumors Unit, IRCCS Istituto Romagnolo per lo Studio dei Tumori (IRST) "Dino Amadori", Meldola (FC), Italy. [5]Pathology Unit, Morgagni-Pierantoni Hospital, AUSL Romagna, Forlì, Italy. [6]Department of Medical Oncology, IRCCS Istituto Romagnolo per lo Studio dei Tumori (IRST) "Dino Amadori", Meldola (FC), Italy. [7]Biosciences Laboratory, IRCCS Istituto Romagnolo per lo Studio dei Tumori (IRST) "Dino Amadori", Meldola (FC), Italy. [8]Department of Pharmacology and Physiology, Drexel University College of Medicine, Philadelphia, PA, USA. [9]Department of Pathology, Helen F. Graham Cancer Center and Research Institute, Christiana Care Health, Newark, DE, USA. [10]Helen F. Graham Cancer Center and Research Institute, Christiana Care Health, Newark, DE, USA. [11]Department of Urology and Department of Pharmacology and Therapeutics, Roswell Park Comprehensive Cancer Center, Buffalo, NY, USA. [12]Department of Pharmacology, Physiology and Cancer Biology, Sidney Kimmel Comprehensive Cancer Center, Thomas Jefferson University, Philadelphia, PA, USA. ✉email: mperego@wistar.org

Received: 15 May 2026 Revised: 31 July 2026 Accepted: 19 August 2026
Published online: 1 September 2026

regulation [31] via recognition of two membrane-bound G protein-coupled receptors, NMUR1 and NMUR2 [32]. However, the heightened levels of NMU found in various tumor types [33] point to additional roles of this pathway in the cancer-neuronal interface [34], potentially modulating the immune-inflammatory microenvironment of tumor growth [35].

In this study, we explored mechanisms of reprogramming of the NEPC microenvironment with actionable therapeutic potential.

MATERIALS AND METHODS

Patient material

A fully de-identified cohort of 5 patients (age 68–72) with histologic diagnosis of high-grade prostatic intraepithelial neoplasia (PIN) was analyzed for differential expression of NMU and $CD8^+$ T cell infiltration by IHC. A second cohort of 11 patients with histologically confirmed diagnosis of NEPC ($n = 2$) or prostate AdCa ($n = 9$) was also evaluated for NMU expression by IHC and blindly for treatment intensity by independent pathology review (Supplementary Table 1). Patients were enrolled in the IRSTB073 biomarker prospective multicenter study (protocol code 0004169/2017), with approval date from the Romagna Ethics Committee (CEROM) of June 15, 2017. The protocol was approved by the Institutional Review Board of IRCCS Istituto Romagnolo per lo Studio dei Tumori (IRST) "Dino Amadori," Meldola, Italy. The study was conducted in compliance with the Declaration of Helsinki and the Good Clinical Practice Guidelines of the International Conference on Harmonization, and written informed consent was obtained from all patients. Commercially available TMA PR633a, BC19021a and BC19012 comprising tissue samples of normal prostate ($n = 11$), prostate AdCa ($n = 115$), benign prostatic hyperplasia (BPH, $n = 6$), PIN ($n = 42$), NEPC ($n = 2$) and cancer-adjacent tissues ($n = 16$) were purchased from TissueArray.Com (Derwood, MD 20855, USA). TMA slides were stained for NMU expression and quantified for the percentage of NMU^+ cells and NMU staining intensity by blind pathology review (IHC score, 0, 1, 2, 3). Image acquisition and human sample pathology assessments were conducted without knowledge of clinical or experimental outcomes.

Cells and cell culture

Human prostate cancer PC3 and DU145 cells were obtained from the American Type Culture Collection (ATCC, Manassas, VA) and cultured at 37 °C in a humidified 5% CO_2 incubator following the supplier's recommendations. Mouse prostate cancer MPten1 and MP3098 cells were the generous gift of Dr. Marcus Ruscetti (UMASS Chan Medical School, Worcester, MA). Cell line identity was verified by short tandem repeat (STR) profiling, and all cell lines were routinely tested and confirmed to be free of Mycoplasma contamination before use.

Cell Toxicity assays with Tasquinimod

In some experiments, prostate cancer cell lines were seeded in 96-well plates at 5×10^3 cells per well in 100 µl of complete medium overnight. The following day, cells were treated with increasing concentrations (0, 0.5, 1, 10, or 20 µM) of Tasquinimod (MedChemExpress) and cell viability was assessed after 72 h using the CellTiter-Glo® Luminescent Cell Viability Assay (Promega), according to the manufacturer's instructions. This experiment was performed 3 times with 3 technical replicates each, one representative is shown.

PMN isolation

Mouse PMN were isolated from spleens of tumor-free (naïve) mice by mechanical dissociation, ACK red blood cell lysis, and positive selection with anti-Ly6G magnetic microbeads (Miltenyi) using two sequential MS column separations according to the manufacturer's instructions. *Human* PMN were isolated from peripheral blood of healthy adult donors recruited through The Wistar Institute Blood Donor Support Core under a Research Compliance-approved protocol (#21812312) by Histopaque® 1119/1077 density gradient centrifugation, followed by ACK lysis and anti-CD15 magnetic bead enrichment (Miltenyi). Purified PMN were counted and used for functional assays.

Mouse strains

C57BL/6-Tg(TRAMP)8247Ng/J (TRAMP) mice were purchased from Jackson Laboratories (Bar Harbor, ME), and animal colonies were maintained and genotyped at The Wistar Institute Animal Facility, following the supplier's specifications and used between 10 and 45 weeks of age. Six-to-eight-week-old C57BL/6J mice were purchased from Charls River Laboratories (Wilmington, MA) and used in xenograft studies. NSG mice were provided by Wistar Animal Facility Shared Resources. Only males were used since prostate cancer only affects male subjects. Mice were randomized by weight before tumor injection or before treatment.

Animal studies

All procedures complied with the recommendations of the *Guide for the Care and Use of Laboratory Animals* issued by the National Institutes of Health (NIH) and were approved by the Institutional Animal Care and Use Committee (IACUC, #201129 approval number) of The Wistar Institute. No formal a priori power calculation was performed. Sample sizes (4–8 mice per group) were selected based on previous experience with these experimental models, animal availability, and the reproducibility of the observed phenotypes. Across independent experiments, these models have demonstrated consistent responses with low variability, allowing biologically meaningful differences to be reliably detected using the indicated group sizes. O (already written in the animal strain section). Mice were randomized by weight before beginning the experiments and no data were excluded from our analysis. For Tasquinimod monotherapy (to inhibit S100a9 alarmin), TRAMP mice received 30 mg/kg Tasquinimod in the drinking water from 15 to 20 weeks of age (5 weeks total), after which treatment was discontinued and mice were monitored until 32 weeks. A total of 7 mice were enrolled in the Tasquinimod single treatment group and 6 mice received vehicle control. For sequential combination with ICI therapy, mice received 15 mg/kg Tasquinimod from 20 to 25 weeks of age (5 wks then discontinued), followed by anti-PD-1 antibody (10 mg/kg, twice weekly, i.p.) from 32 to 37 weeks of age. Control mice received an isotype-matched antibody on the same schedule. Animals were monitored until 42–45 weeks of age. 8 received the combined sequential treatment, 5 mice received only Tasquinimod and isotype control, and 4 mice received only ICI therapy. For prostate cancer xenografts, 5×10^5 MPten-1 cells (pIKO or ShNMU $n = 5$ each for tumor growth and $n = 6$ PLKo and 7 ShNMU for flow cytometry) were then injected s.c. onto the right flank of male C57BL/6J mice in 200 µl total volume (1:4 dilution with growth factor-reduced Matrigel®, Corning). Animals were examined every other day, and tumor size was measured with a caliper three times per week for tumor growth. For ICI therapy, 5 mice per group were enrolled in the study. Prostate tumors harvested at the end of the experiments were mechanically dissociated and enzymatically digested with mouse tumor dissociation kit (Miltenyi Biotec) following manufacturers' instruction. Blinding was applied where feasible. While not all in vivo experiments were performed under blinded conditions, image acquisition and IHC quantification were performed by investigators blinded to experimental groups. Selected flow cytometry analyzes were also performed blinded to group allocation.

T cell suppression assay

Mouse or human PMN isolated as above where co-cultured at graded ratios (2:1; 1:1, 1:2, 1:4, 1:8) with CellTrace™ Violet-labeled total splenocytes or T cells harvested from naïve mice (1×10^5), according to the manufacturer's instructions (Thermo Fisher Scientific). T cells were isolated from naive mouse spleen by $CD8^+$ T cell Isolation Kit (Miltenyi biotechnology) according to manufacturers' instructions and stimulated by incubation with plate-bound antibodies to CD3 and CD28 (BioLegend). Human PMN were incubated at ratios of 2:1, 1:1, 1:2, 1:4 with CellTrace™ Violet–labeled human PBMCs isolated from whole blood (1×10^5) and T cell activation was induced using Cell Activation Cocktail (BioLegend). After 48 h, T cell proliferation in the presence of PMN co-culture was assessed by CellTrace™ dilution in $CD8^+$ T cells via flow cytometry. All assays were performed in 96-well U-bottom plates. When indicated, PMN were pre-cultured 6 h in with NMU (100 nM) or vehicle for 6 h, then washed to remove NMU, counted and plated with splenocytes. Suppression assays were performed 3 times (for humans with different healthy donors) with 3 technical replicates each.

Migration assays

Mouse or human PMN (0.5×10^5) isolated as described above, were suspended in 500 µl of RPMI medium supplemented with 10% FBS were placed in Transwell inserts (0.8 µm pore size) within 24-well plates containing 500 µl of same medium in the lower chamber. Recombinant

NMU (100 nM) was added to the upper chamber for inhibition studies, cells were incubated with increasing concentrations (0–10 μM) of SB-255610, a small-molecule competitive antagonist of CXCR2 (CXCR2i, Selleck Chemicals). After 6 h, migrated cells in the bottom chamber were harvested and viable cells were quantified by light microscopy. In some experiments, conditioned medium (CM) harvested from MPten-1 cells was used as a source of chemoattractant. For these experiments, MPten-1 cells were transfected with ON-TARGETplus non-targeting control or mouse/human Nmu siRNAs (Horizon) according to the manufacturer's instructions. After 24 h, conditioned media were collected, cleared by centrifugation, and used in Transwell migration assays. Migration assays were performed 3 times (for humans with different healthy donors) with 3 technical replicates each.

NMU silencing

For transient NMU silencing, MPten-1 cells were transfected with ON-TARGETplus non-targeting control or mouse/human Nmu siRNAs (Horizon). Cells were seeded at 2×10^5 cells per 3 ml in 6-well plates and incubated for 16 h at 37 °C prior to transfection. Lipofectamine 2000 complexes were prepared by separately incubating Mix A (2 μl Lipofectamine 2000 in 150 μl Opti-MEM™ per well) and Mix B (3 μl of 10 μM siRNA in 150 μl Opti-MEM™ per well) for 5 min at room temperature, followed by mixing and incubation for an additional 25 min to allow complex formation. The siRNA-lipid complexes were then added dropwise to cells and incubated for the indicated time points. For *stable shRNA-mediated silencing of NMU*, MPten-1 cells were transduced with scramble control or NMU shRNA lentiviral vectors (VectorBuilder Chicago, IL; Vector IDs: VB010000-0009mxc and VB240620-1413err, respectively) according to manufacturer's protocol. Transduced cells were selected with puromycin (2 μg/ml) and maintained under standard culture conditions.

ELISA

Mouse blood was collected into heparinized tubes, and plasma was isolated by centrifugation ($200 \times g$, 10 min at 4 °C) and stored at −80 °C until analysis. Plasma S100A9 (from 12 mice 10–15 wks and $n = 14$ 17–22wk old mice) and NMU levels (3 10–15wks old, 3 17–22wks,4 23–29wks and 9 30–30wks old mice) were quantified using commercial ELISA kits (R&D Systems DY8596-05 and Cusabio CSB-EL015902MO, respectively) according to the manufacturers' instructions. Absorbance was measured using a Promega™ GloMax® Plate Reader.

Immunohistochemistry (IHC)

Samples stained at Wistar Histotechnology facility: Prostate tissues were fixed in 10% neutral buffered formalin for 16 h, paraffin embedded, and sectioned at 5 μm. After deparaffinization and rehydration [xylene (6 min), xylene substitute (6 min), 100% ethanol (2 min twice), 95% ethanol (2 min twice), and distilled water (1 min)], antigen retrieval was performed in DAKO EDTA buffer using a pressure cooker (20 min, 95 °C). Sections were permeabilized with 0.1% Triton X-100 (15 min at 22 °C), blocked with 2.5% horse serum (45 min at 22 °C), and incubated overnight at 4 °C with primary antibodies against CD8α (D4W2Z, Cell Signaling Technology), Ly6G (E6Z1T, Cell Signaling Technology), CD31/PECAM-1 (D8V9E, Cell Signaling Technology), and NMU (#24862-1-AP, Thermo Fisher Scientific) incubated at 1:200 dilution for 16 h at 4 °C. After incubation with HRP-conjugated horse anti-rabbit IgG polymer (1:200) for 30 min at 22 °C, signal was developed with DAB for 90 sec, followed by hematoxylin counter-staining. NSE was detected by NSE Polycklinal antibody (1:200, PeproTech) according to manufacturer's instructions (4 tumors were stained for each group). Images were acquired using a Nikon 80i microscope or NanoZoomer S60 digital slide scanner (Hamamatsu), and quantitative analysis was performed using QuPath software. *Sample stained at IRST*: Automated IHC was performed on 3-μm FFPE tissue sections using the Ventana Benchmark ULTRA automated staining platform (Ventana Medical Systems, Tucson, AZ, USA). NMU staining (Invitrogen, PA5-96566) was detected with the OptiView DAB Detection Kit, while CD8 (Roche, clone SP239, cat#5937248001) was evaluated by sequential dual staining using DAB and AP Red chromogens achieved with the OptiView DAB Detection Kit and the ultraView Universal Alkaline Phosphatase Red Detection Kit, respectively (Ventana Medical Systems). Sections were counterstained with Hematoxylin II (Ventana Medical Systems), and whole-slide images were acquired at ×40 magnification using an Aperio CS2 scanner (Leica Biosystems, Nussloch, Germany). NMU expression was quantified as the percentage of positive tumor cells, and $CD8^+$ lymphocytes were quantified as the number of positive cells per high-power field (HPF, ×40) by trained pathologist.

Western Blot analysis

The various mouse and human cell types were lysed in RIPA buffer supplemented with phosphatase inhibitors (Roche). Protein concentration was determined by Bradford assay (Bio-Rad), and 40 μg aliquots of total protein were resolved on 10% NuPAGE polyacrylamide gels (Thermo Fisher Scientific) in MOPS running buffer. Proteins were transferred onto PVDF membranes using a wet transfer system with 1× transfer buffer (Thermo Fisher Scientific). Membranes were blocked in 5% non-fat milk for 1 h at 22 °C and incubated for 16 h at 4 °C with primary antibodies against NMU (#24862-1-AP, Thermo Fisher Scientific) or vinculin (E1E9V, Cell Signaling Technology) diluted in PBS containing 1% BSA (Sigma). After washing in TBS-T, membranes were incubated with HRP-conjugated secondary antibody of appropriate specificity (1:1000) in 5% milk for 2 h at 22 °C (Supplementary Table 2). Signal detection was performed using Clarity™ Western ECL substrate (Bio-Rad), and chemi-luminescence was captured on Amersham Hyperfilm ECL using a Konica SRX-101A developer.

RT-qPCR

Cells were lysed in RNA lysis buffer from the Quick-RNA Microprep Kit (Zymo Research), and lysates were stored at −80 °C until RNA extraction using the same kit. cDNA synthesis was performed using the High-Capacity cDNA Reverse Transcription Kit (Thermo Fisher Scientific) in the presence of RNase inhibitor. The RT-qPCR amplification reaction was carried out using Applied Biosystems™ PowerUp™ SYBR™ Green Master Mix (Thermo Fisher Scientific) using primer sequences listed in Supplementary Table 3. Amplification reactions were carried out on a Bio-Rad thermocycler or a QuantStudio™ 5 Real-Time PCR system (Thermo Fisher Scientific). qPCR for PMN RNAseq validation was performed with PMN coming form 4 different mice with experimental triplicates.

RNA-seq

Mouse prostate tissue samples were harvested from 12- or 19-week-old TRAMP mice ($n = 3$ per group) and snap-frozen in liquid nitrogen. Reads were aligned to the mm10 mouse genome using STAR [36], and gene expression was quantified with RSEM (Ensembl GRCm38.89 annotation) [37]. Differential gene expression was analyzed from raw counts using DESeq2, with significance defined as a false discovery rate (FDR) < 0.05. Gene expression was visualized using heatmaps of DESeq2-normalized counts [38]. RNA-seq data are available in the NCBI GEO database (GSE33830). For RNAseq on isolated PMN, PMN were isolated from spleens of C57BL/6 J mice, incubated with recombinant NmU (100 nM) for 16 h at 37 °C, harvested in RNA Lysis Buffer (Zymo) and stored at −80 °C until processing.

Flow cytometry

Tissues harvested from TRAMP mice were collected, and spleens were mechanically dissociated through a 70 μm filter (VWR International). Prostate tissues and subcutaneous MPten-1 tumors were minced and enzymatically digested into single-cell suspensions using a Tumor Dissociation Kit (Miltenyi Biotec) following the manufacturer's protocol. All cell suspensions were filtered, and erythrocytes were lysed with ACK buffer. Cells were stained in Brilliant Stain Buffer (BD) with 50 μl of antibody mix per sample (Supplementary Table 4) and Zombie UV LIVE/DEAD™ viability dye (1:300) for 15 min at 4 °C, then washed with MACS buffer (1% FBS, 5 mM EDTA in PBS). Intracellular staining for T cells (FOXP3, KI67, TCF-1, GrzB) was achieved using eBioscience™ Foxp3 / Transcription Factor Staining Buffer Set, according to the manufacturer's instructions. Intracellular PMN S100a9 staining used the Cytofix/CytoPerm kit (BD Biosciences) was detected following the manufacturer's protocol with a 15-min incubation period at 4 °C. NMUR1 primary surface staining 30 min at 4 °C was followed by secondary anti-mouse Alexa488 antibody (Thermo Fisher Scientific) for 30 min at 4 °C. SV40 and Ctrl Tetramers were kindly provided by NIH Tetramer Core Facility at Emory. Compensation controls were set using UltraComp eBeads™ and ArC™ Amine Reactive Compensation Beads. Samples were acquired on a BD FACSymphony™ cell analyzer, and data were analyzed using FlowJo™ v10.7 (Tri-Star). A complete list of antibodies used for flow cytometry studies is provided in Supplementary Table 4. Sample size for flow is indicated in the figure legend.

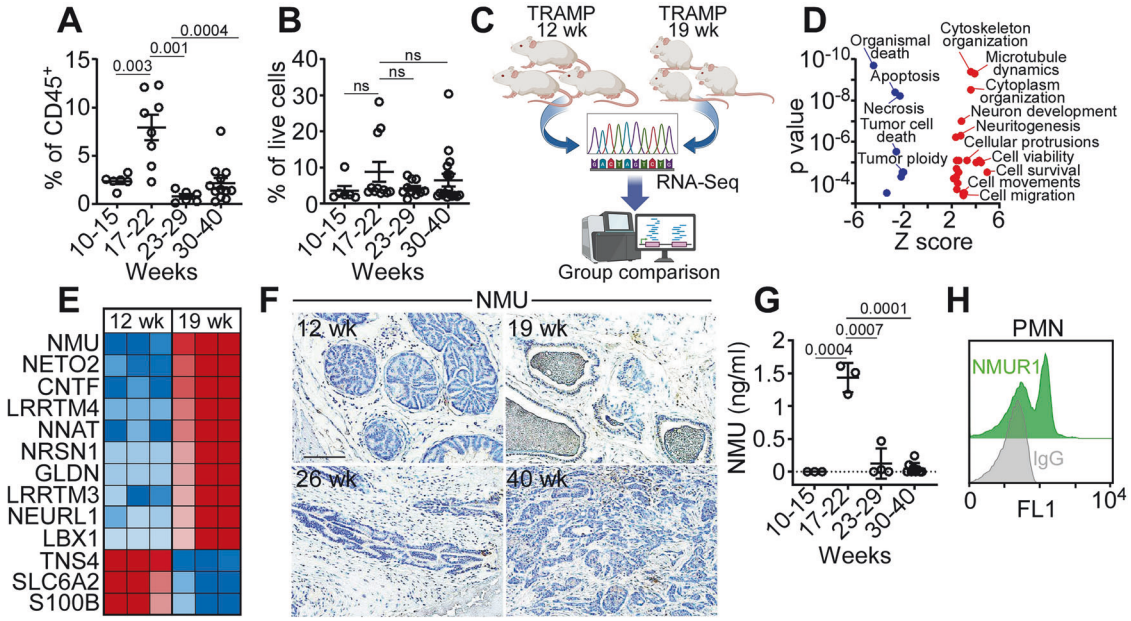


Fig. 1 Reprogramming of the prostate immune microenvironment during NEPC progression. Prostate (**A**) or spleen (**B**) tissue samples harvested from TRAMP mice at the indicated ages were analyzed for the presence of Ly6G$^+$ PMN by flow cytometry. Each symbol is an individual mouse determination. **C** Schematic diagram of RNA-Seq profiling of prostate tissue samples from TRAMP mice of the indicated age groups. **D** Volcano plot of differentially modulated pathways in TRAMP mice at 19 *vs*. 12 weeks of age by RNA-Seq and Ingenuity Pathway Analysis (IPA). **E** The conditions are as in (**C**) and differentially modulated neuronal regulators in 19- *vs*. 12-week-old TRAMP mice are shown in a heatmap ($n = 3$). For all regulators, $p < 0.05$; FDR < 5%. For **D**, **E**, Blue, downregulated; red, upregulated. **F** Prostate tissue samples collected from TRAMP mice at the indicated ages (wk, week) were analyzed for NMU expression by immunohistochemistry (IHC). Representative images. Scale bar, 100 µm. **G** Plasma samples collected from TRAMP mice at the indicated ages were analyzed for NMU levels, by ELISA. Each symbol is an individual mouse determination. Mean ± SD (n = 3–6). For **A**, **B**, **G**, numbers are *p* values by unpaired, two-sided *t* test. **H** PMN isolated from the spleens of C57BL/6J mice were incubated with non-binding IgG or an antibody to the type I NMU receptor (NMUR1) and analyzed by flow cytometry. Representative experiment.

RESULTS

NMU modulation of NEPC immune microenvironment

To begin elucidating mechanisms of immune rewiring of the prostate cancer microenvironment, we looked at early stages of tumor formation in Transgenic Adenocarcinoma of the Mouse Prostate (TRAMP) mice. In this model, transgenic expression of the SV40 large T antigen oncogene in the prostate induces high-penetrance, stepwise prostate cancer formation, predominantly with neuroendocrine histology [39]. Prostate tissues harvested from 17 to 22-week-old TRAMP mice, a time frame corresponding to the formation of high-grade prostatic intraepithelial neoplasia (PIN), exhibited extensive accumulation of Ly6G$^+$ polymorphonuclear neutrophils (PMN) by flow cytometry (Fig. 1A). In contrast, earlier (10–15 weeks) or later (23–40 weeks) stages of TRAMP tumorigenesis were unaffected (Fig. 1A). These changes were specific to the prostate microenvironment because no differences in the accumulation of Ly6G$^+$ PMN were observed in spleens of TRAMP mice at any age examined (Fig. 1B). Coinciding with PMN recruitment, prostate tissues of TRAMP mice at 17–22 weeks exhibited reduced accumulation of CD3$^+$ T cells compared to 10–15- or 23–40-weeks of age, by flow cytometry (Fig. S1A). Subset analysis demonstrated that both CD4$^+$ and CD8$^+$ T cells were reduced in these settings, compared to other time intervals of TRAMP tumor formation (Fig. S1A).

Based on these results, we next compared the transcriptome of prostate tissues harvested from TRAMP mice at 12- *vs*. 19-weeks of age, by RNA-Seq (Fig. 1C). We found that 19-weeks-old TRAMP mice upregulated multiple pathways of cell survival, cell motility and neuronal development that were not present at earlier stages of prostatic oncogenesis in 12-weeks-old mice (Fig. 1D). This was accompanied by increased expression of key regulators of cell proliferation and cell survival (ERBB2, RABL6, CCND1, E2F1), cytoskeletal rearrangement (CKAP2L) and PMN activation (CSF2) (Fig. S1B). Conversely, pathways of tumor cell death (Fig. 1D) and tumor suppression (TP53, CDKN1A, CDKN2A, RB, RBL2) were downregulated, compared to the 12-week-old mouse group (Fig. S1B).

Consistent with transition to a neuroendocrine phenotype, 19-weeks-old TRAMP mice also exhibited heightened expression of regulators of synaptic plasticity (NEURL1, LRRTM4, LRRTM3, NETO2), neuronal differentiation (LBX1, NNAT, GLDN), and neurotrophic responses (NETO2, NMU) (Fig. 1E). The top hit in this analysis was NMU (Z Score=4.34; FDR < 5%; $p = 3.62 \times 10^{-9}$), a 25-amino acid neuropeptide with multiple functions in cellular homeostasis [30].

By immunohistochemistry (IHC), NMU was undetectable in prostate tissues of TRAMP mice at 12-weeks of age, became expressed in the prostatic epithelium by 19 weeks and remained present, albeit at heterogeneous levels, in 26- and 40-week-old animals (Fig. 1F). Plasma levels of NMU were also upregulated in 17–22-week-old TRAMP mice, compared to other age groups, by ELISA (Fig. 1G), and PMN isolated from TRAMP mice expressed high levels of the NMU type 1 receptor, NMUR1 [32], by flow cytometry (Fig. 1H), potentially suggestive, albeit not conclusively of pathway response.

Differential NMU expression in human primary and metastatic prostate cancer

When analyzed in the cohort of prostate cancer patients of the TCGA dataset (PRAD), high expression of NMU correlated with markers of cell proliferation (MKI67), mitotic progression (STMN1) and DNA synthesis (TOP2A), whereas regulators of actin dynamics (ACTA1, NRAP, XIRP2) were downregulated (Fig. S1C). In addition, high NMU levels correlated with oncogene expression, including Myc, E2F and mTORC1 (Fig. S1D). In line with neuroendocrine

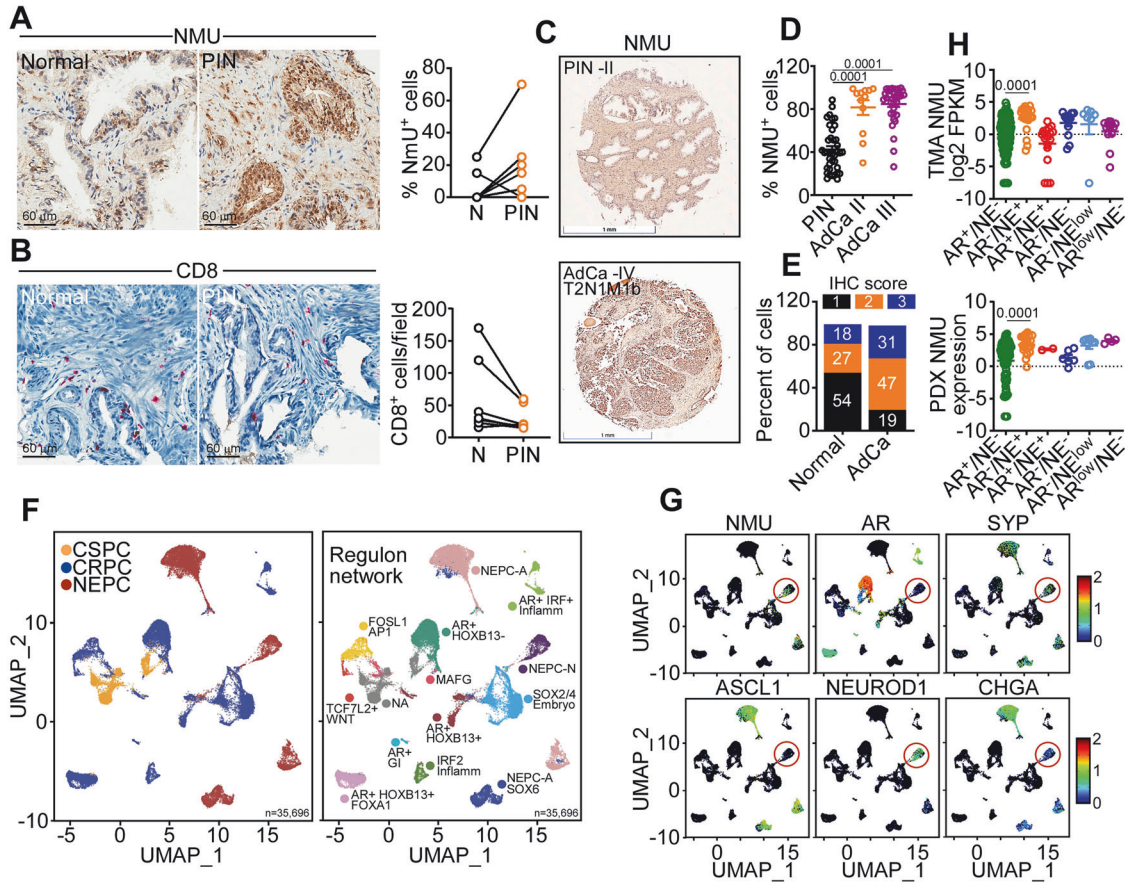


Fig. 2 NMU expression in human prostate cancer. Tissue sections from normal prostate or high-grade PIN were analyzed for NMU expression (**A**) or $CD8^+$ cells (**B**), by immunohistochemistry (IHC). Right, IHC quantification of six independent cases. Each point is an individual patient sample. Scale bars, 60 µm. Representative images. **C** Representative TMA images of PIN (top) or prostate adenocarcinoma (AdCa, bottom) were analyzed for NMU expression by IHC. The grade, stage and TNM classification are indicated. Scale bars are indicated. **D, E** The conditions are as in **B** and the percentage of NMU+ cells (**D**) and NMU staining intensity (1+/2+/3+) (**E**) was quantified. The percentage of cells with each staining intensity is indicated. AdCa, $n = 98$; Normal, $n = 11$. **F** UMAP visualization of tumor cells from human prostate cancer scRNA-seq dataset GSE264573 [40], colored by tumor subtype annotation (left). CSPC, castration sensitive; CRPC, castration resistant; NEPC, neuroendocrine. Tumor populations with distinct gene regulatory (regulon) networks [40] are shown (right). NA, not available for castration sensitive tumors. **G** Feature plots showing normalized gene expression of NMU and the indicated lineage-associated markers across tumor cell states. **H** Biopsies of metastatic CRPC from the Rapid Autopsy Program of the University of Washington (GSE126078) [41] and arranged in a TMA (top) or propagated as patient-derived xenografts (PDX) (bottom) were analyzed for differential NMU expression. Each point is a patient determination. AR, androgen receptor, NE, neuroendocrine. Numbers are *p* values by unpaired, two-sided *t* test.

transition, an androgen response gene signature was down-regulated in NMU-high PRAD (Fig. S1D).

Consistent with the results obtained with TRAMP mice, NMU was also highly expressed in a cohort of human PIN lesions, compared to normal epithelium, by IHC (Fig. 2A), correlating with reduced intraprostatic accumulation of $CD8^+$ T cells, by IHC (Fig. 2B). Therefore, we next examined the expression of NMU in multiple independent tissue microarrays (TMA) representative of the spectrum of prostatic tumorigenesis (Supplementary Table 1). In this analysis, NMU was prominently expressed in PIN ($42.3 \pm 3.2\%$ NMU+ cells, $n = 38$) as well as stage II ($81.5 \pm 6.7\%$ NMU+ cells, $n = 12$) and stage III ($84.8 \pm 2.9\%$ NMU+ cells, $n = 34$) prostate adenocarcinoma by IHC (Fig. 1C, D). Two cases of NEPC contained 82% NMU+ cells with 1+/2+ staining intensity, by IHC. Blind pathology scoring of the aggregate TMA staining revealed high NMU staining intensity (2+/3+) in 78% of AdCa cases ($n = 98$), compared to normal prostate (Fig. 1E). To further assess the clinical relevance of NMU expression in NEPC, we next analyzed publicly available single-cell RNA-seq dataset GSE264573 (Fig. 2F) from patients with advanced prostate cancer [40]. Tumor cell-specific analysis revealed that NMU expression was detected in differentiated NEPC enriched for ASCL1, SYP, CHGA and NEUROD1 transcriptional regulon activity (Fig. 2G). Next, we examined the expression of NMU in biopsies of metastatic castration-resistant prostate cancer (mCRPC) collected under the Rapid Autopsy Program at The Prostate Cancer Biorepository Network at the University of Washington (GSE126078) [41], maintained as TMA or patient-derived xenografts (PDX). In this cohort, NMU was prominently expressed in biopsies of metastatic prostate cancer (Fig. 2H, top) as well as related PDX samples (Fig. 2H, bottom), with higher levels in AR-independent (AR^-/AR^{low}) and neuroendocrine-associated (NE^+) subtypes compared to AR-high (AR^+) tumors (Fig. 2H).

Differential expression of NMU in cancer

We next asked whether increased expression of NMU was unique to prostate cancer. Analysis of public databases revealed that NMU protein levels were elevated in multiple, genetically unrelated tumor types (Fig. S2A). In addition, high levels of NMU correlated with shortened patient survival in malignancies of breast, ovary, lung, stomach and multiple myeloma (Fig. S2B), also known for the presence of rarer, but highly aggressive and rapidly metastatic neuroendocrine variants [42, 43]. Similarly, NMU (Fig. S2C), but not its receptor NMUR1 (Fig. S2D), was over-expressed in most human

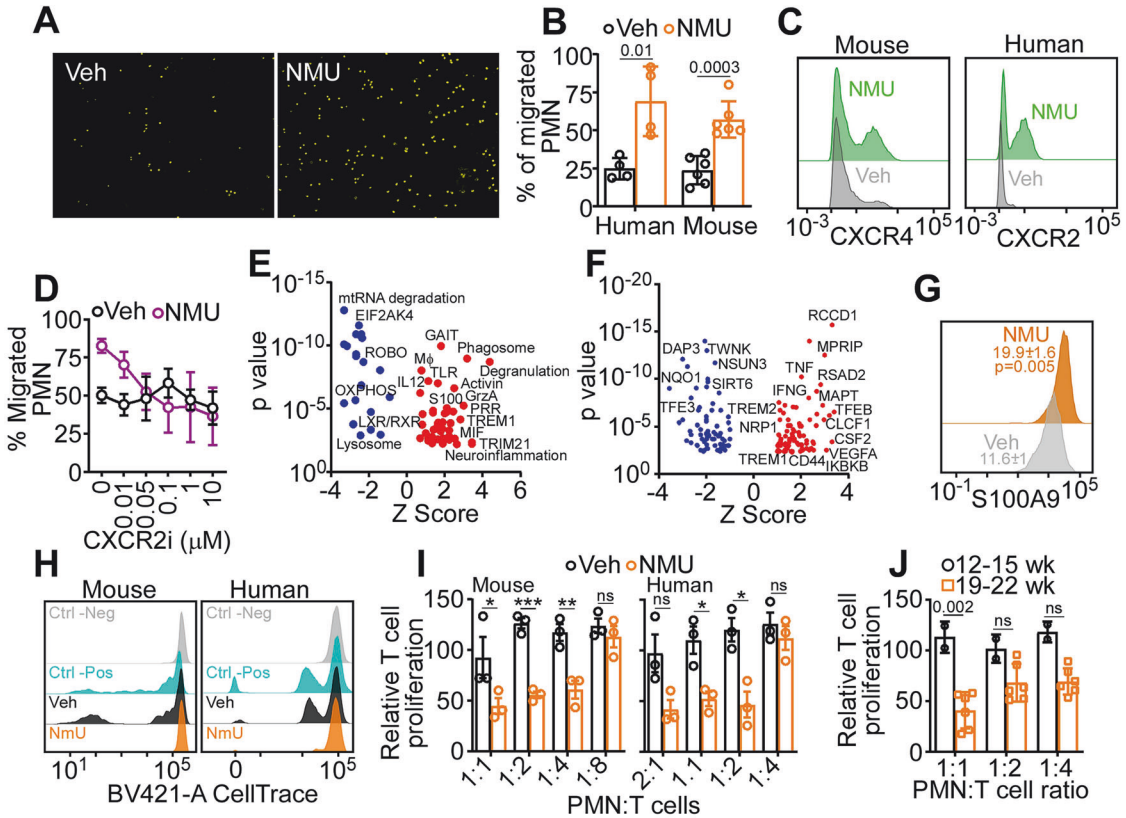


Fig. 3 NMU regulation of PMN functions. Human or mouse (C57BL/6J) PMN were incubated with vehicle (Veh) or recombinant NMU and DAPI-stained nuclei of migrated PMN through a Transwell membrane (**A**) were quantified (**B**). Mean ± SD ($n = 4$, human PMN; $n = 6$, mouse PMN). **C** Mouse or human PMN were incubated with vehicle (Veh) or recombinant NMU and analyzed for differential cell surface expression of CXCR4 (left) or CXCR2 (right) by flow cytometry. Representative experiment. **D** Mouse PMN treated with vehicle (Veh) or recombinant NMU were incubated with SB-265610, a small molecule competitive inhibitor of CXCR2 (CRXCR2i) and analyzed for cell migration in transwell assays. Mean ± SD ($n = 3$). Mouse PMN stimulated with recombinant NMU for 6 h were analyzed for changes in gene expression by RNA-Seq and modulation of *Pathways* (**E**) or *Effectors* (**F**) identified by Ingenuity Pathway Analysis (FDR < 5%; $p < 0.05$) were visualized in volcano plots. Blue, downregulated; red, upregulated. **G** Mouse PMN were incubated with vehicle (Veh) or recombinant NMU and changes in expression of intracellular S100A9 were analyzed by flow cytometry. Numbers are fluorescence GeoMean ± SEM ($n = 4$). Mouse or human PMN stimulated with vehicle (Veh) or recombinant NMU were incubated at various ratios with CellTrace™ Violet-labeled mouse splenocytes or -human PBMC, respectively, and CD3/CD28-stimulated T cell proliferation was determined by flow cytometry (**H**, representative experiment) and quantified (**I**). Mean ± SEM ($n = 3$) **J** The experimental conditions are as in (**H**, **I**) except that mouse T cells were mixed at various ratio with PMN isolated from TRAMP mice at the indicated ages before quantification of T cell proliferation by CellTrace™ staining and flow cytometry. Mean ± SD ($n = 2$–6). For panels (**B**, **I**, **J**), each symbol is an individual mouse determination. Numbers are p values by unpaired, two-sided t test. *$p = 0.04$-0.01; **$p = 0.005$; ***$p = 0.0005$; ns, not significant.

tumor cell lines in the Cancer Cell Line Encyclopedia. Although copy number was unchanged, both NMU and NMUR1 were identified as selected dependency genes in RNAi/CRISPR screens of tumor cells (Fig. S2E). Consistent with a role of this pathway in immune reprogramming of the microenvironment, high levels of NMU correlated with reduced infiltration of $CD8^+$ T cells in multiple tumor types, including prostate, pancreatic and stomach adenocarcinoma, as well as uterine cancer, uveal melanoma and testicular germ cell tumor (Fig. S2F). In certain malignancies, a reduction in $CD8^+$ T cells in NMU-high tumors correlated with increased accumulation of myeloid cells (Fig. S2F), resistance to immunotherapy and shortened patient survival (Fig. S2B).

NMU regulation of microenvironment inflammation

Next, we looked at the effect of NMU on tumor-associated responses in the microenvironment. First, increasing concentrations of recombinant NMU did not affect the viability of mouse prostate cancer MPten-1 cells (Fig. S3A), which express cell surface NMUR1, by flow cytometry (Fig. S3B). Reciprocally, stable shRNA silencing of NMU did not modulate MPten-1 cell proliferation (Fig. S3C) or single-cell clonogenic ability (Fig. S3D). Conversely, recombinant NMU potently stimulated human or mouse PMN migration across Transwell inserts (Fig. 3A, B). A similar response was observed with PMN isolated from different sources, including spleen or bone marrow (BM) of C57BL/6 J mice (Fig. S3E). Furthermore, conditioned medium from prostate cancer MPten-1 or MP3098 cells silenced for NMU by siRNA had reduced ability to support PMN migration in Transwell assays (Fig. S3F). Mechanistically, NMU stimulation of PMN migration was associated with increased cell surface expression of the chemokine receptors, CXCR4 and CXCR2, by flow cytometry (Fig. 3C), and incubation with SB-265610, a small molecule competitive inhibitor of CXCR2 (CXCR2i), suppressed the increase in PMN migration mediated by NMU (Fig. 3D).

We used RNA-Seq to profile gene expression changes in PMN exposed to NMU. We found that NMU stimulation induced extensive transcriptional changes in PMN (Fig. S3G), with upregulation of pathways implicated in myeloid activation, host defense/innate immunity (PRR, TLR, GRZA, IL7), inflammation (TREM1, MIF, S100, IL12, GAIT), and cell motility (TORC1, NF1/RAS) (Fig. 3E). In contrast, pathways of mitochondrial oxidative phosphorylation and nucleic acid processing, lysosomal functions

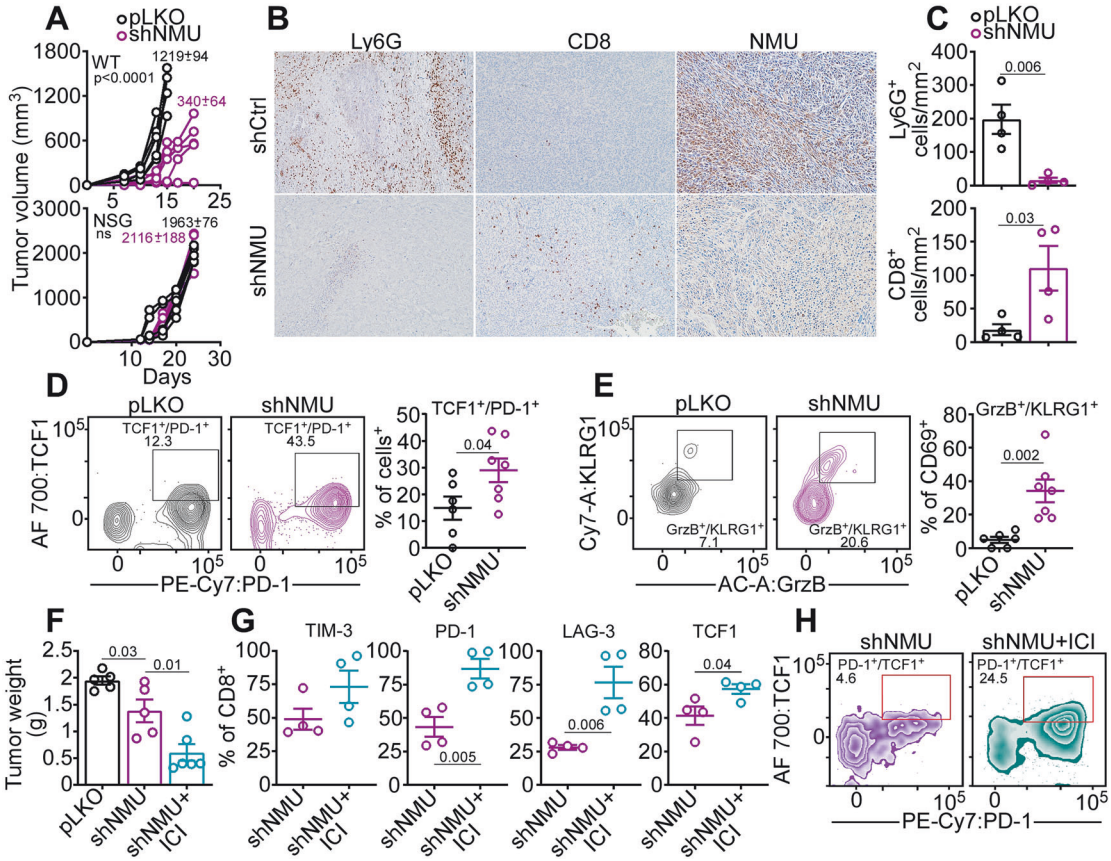


Fig. 4 NMU regulation of NEPC growth. A Mouse MPten-1 cells stably expressing pLKO or NMU-directed shRNA (shNMU) were engrafted onto the flanks of C57BL/6J (top) or immunodeficient NSG (bottom) mice (5 animals/group) and tumor growth was quantified at the indicated time intervals with a caliper. Numbers correspond to average tumor volumes at the end of the experiment. A *p* value is indicated. ns, not significant. **B**, **C** The conditions are as in (**A**, top) and MPten-1 tumors grown in WT C57BL/6J mice were harvested at the end of the experiment and analyzed for intratumoral accumulation of Ly6G$^+$ PMN, CD8$^+$ T cells or NMU, by IHC (**B**) and quantified (**C**). Mean ± SEM ($n = 4$). Scale bar, 200 µm. Representative images. **D, E** MPten-1 tumors as in (**A**, top) were analyzed for modulation of specialized T cell subsets, TCF1$^+$/PD-1$^+$ (**D**) and GrzB$^+$/KLRG1$^+$ (**E**) by multiparametric flow cytometry (left, representative plots) and quantified (right). The percentage of positive cells is indicated. Mean ± SEM ($n = 6$–7). **F** C57BL/6J mice carrying syngeneic MPten-1 tumors expressing pLKO or shNMU as in (**A**, top) were treated with an antibody to PD-1 (ICI) and tumor weight in the indicated mouse groups was quantified at the end of the experiment (day 13 from engraftment). Mean ± SEM ($n = 5$–6). **G** The conditions are as in **F** and MPten-1 tumors with or without ICI treatment were analyzed for differential expression of the indicated CD8$^+$ T cell markers by flow cytometry. Mean ± SEM ($n = 4$). **H** The conditions are as in **F** and tumor samples were analyzed for differential accumulation of PD-1$^+$/TCF1$^+$ CD8$^+$ T cells by multiparametric flow cytometry. The percentage of double positive cells indicated. For **A**, **C**–**G**, each symbol is an individual mouse determination. Numbers are to *p* values by unpaired, two-sided *t* test.

and inhibitory receptors of cell motility (ROBO) were inhibited (Fig. 3E). Consistent with this, bioinformatics analysis of this dataset revealed that NMU upregulated multiple key mediators of inflammation (IFN, TNF, MYD88, STAT1) and cell movements (MAPT, TFEB, CD44, CSF2, NRP1, TREM2, CCL20, MPRIP, IKBKB) in PMN (Fig. 3F). In validation experiments, NMU stimulation of spleen-isolated PMN prominently upregulated a gene signature of inflammation, innate immunity and cell motility, by RT-qPCR (Fig. S3H).

Among the inflammatory mediators upregulated by NMU in PMN was S100A9, a cytokine-like Damage-Associated Molecular Pattern (DAMP), which contributes to myeloid immunosuppression [44]. Accordingly, stimulation of spleen-derived PMN with recombinant NMU was sufficient to increase the levels of intracellular S100A9, by flow cytometry (Fig. 3G). Functionally, NMU-stimulated mouse or human PMN became potently immunosuppressive, inhibiting T cell proliferation induced by CD3/CD28 stimulation, by CellTrace analysis and flow cytometry (Fig. 3H, I). A similar response was observed in TRAMP mice, where PMN harvested from 19 to 22-week-old animals suppressed syngeneic T cell proliferation, compared to PMN harvested from TRAMP mice of 12–15 weeks of age (Fig. 3J). Conversely, PMN isolated from S100A9 knockout mice did not inhibit syngeneic T cell proliferation, by CellTrace analysis and flow cytometry (Fig. S3I).

NMU reprogramming of the immune microenvironment sustains prostate cancer progression

To test the impact of NMU-S100A9 signaling on prostate cancer progression, we next engrafted MPten-1 cells stably expressing pLKO or shNMU onto the flanks of syngeneic WT C57BL/6 mice or immunocompromised NSG mice. In these experiments, depletion of NMU significantly inhibited MPten-1 tumor growth in WT mice (Fig. 4A, top). This response required an intact immune system because NMU silencing had no effect on MPten-1 tumor growth in immunocompromised NSG mice (Fig. 4A, bottom). In addition, MPten-1 tumors depleted of NMU exhibited increased accumulation of CD8$^+$ T cells and a concomitant reduction in Ly6G$^+$ PMN, compared to control animals, by IHC (Fig. 4B, C).

Similar results were obtained by profiling the immune infiltrate of MPten-1 tumors in WT mice by flow cytometry. Here, depletion of NMU reduced the intratumoral accumulation of Ly6G$^+$ PMN (Fig. S4A), while increasing the recruitment of CD8$^+$ but not CD4$^+$

T cells (Fig. S4B). In addition, loss of NMU expanded $CD8^+$ T cell subsets implicated in the response to therapeutic immune checkpoint inhibition (ICI), including 'stem-like' and self-renewing $TCF1^+/PD\text{-}1^+$ (Fig. 4D) and cytotoxic $GrzB^+/KLRG1^+$ T cells (Fig. 4E).

Based on these results, we next asked whether depletion of NMU enhanced the activity of ICI in preclinical models of prostate cancer. In these experiments, the combination of NMU silencing plus systemic administration of an antibody to the immune inhibitory receptor, PD-1 was more effective than either condition alone in suppressing MPten-1 tumor growth in WT C57BL/6 J mice (Figs. 4F and S4C). Compared to NMU silencing alone, the addition of PD-1 blockade increased the intratumoral recruitment of $CD8^+$ T cells with higher levels of activation markers, PD-1, LAG-3 and TIM-3 (Fig. 4G), while also upregulating 'stem-like' $TCF1^+/PD\text{-}1^+$ (Figs. 4H and S4D) and effector resident $CD69^+/KLRG1^+$ T cell subsets (Fig. S4E). These changes were specific because intratumoral $CD4^+$ T cells did not exhibit modulation of activation markers (Fig. S4F) and myeloid (Fig. S4G) or NK cell (Fig. S4H) subsets were unchanged after NMU silencing with or without PD-1 blockade. In addition, no changes in T cell activation markers were observed in $CD8^+$ T cells isolated from the spleen of tumor-bearing animals (Fig. S4I).

Preclinical targeting of NMU-S100A9 signaling in NEPC

Although NMU has not been considered as a therapeutic target, its potential effector of immunosuppression, S100A9 [45], has been evaluated in prostate cancer [46]. Consistent with this notion, PMN from prostate tissues of TRAMP mice of 17–22-weeks of age contained high levels of S100A9 (Fig. S5A). These changes were specific for early TRAMP tumorigenesis because S100A9 was not significantly modulated in prostate samples of younger (10–15 weeks) or older (23–40 weeks) TRAMP mice (Fig. S5A). In addition, plasma levels of S100A9 increased in 17–22-week-old TRAMP mice, compared to 10–15 week-old animals, by ELISA (Fig. S5B). The modulation of S100A9 was restricted to the microenvironment of prostatic tumorigenesis as no changes in S100A9 levels were observed in PMN from the spleens of TRAMP mice at any time point examined (10–40 weeks) (Fig. S5C).

To therapeutically target S100A9, we next treated TRAMP mice with the small molecule inhibitor, Tasquinimod [46]. Systemic administration of Tasquinimod was well-tolerated and significantly inhibited tumor growth in TRAMP mice, compared to controls (Figs. 5A and S5D). Although Tasquinimod has been linked to inhibition of angiogenesis, no appreciable differences in intraprostatic CD31 staining were observed in control or treatment groups by IHC (Fig. S5D). Similar to the effect of NMU silencing, Tasquinimod treatment reduced the accumulation of $Ly6G^+$ PMN in the prostate of TRAMP mice, concomitantly with increased recruitment of $CD8^+$ T cells, by IHC (Fig. 5B, C) and multiparametric flow cytometry of isolated tumor tissues (Fig. S5E). Compared to vehicle-treated animals, $CD8^+$ T cells in Tasquinimod-treated TRAMP mice were tumor antigen-specific, as judged by strong reactivity with an SV40-directed MHC tetramer and flow cytometry (Fig. 5D). In addition, Tasquinimod treatment expanded intraprostatic $CD8^+$ T cell subsets expressing 'stem-like' (TCF1) and cytotoxicity (GrzB) markers, by flow cytometry (Fig. S5F), without affecting the viability of prostate cancer cell types in culture (Fig. S5G).

Finally, we asked if Tasquinimod could also sensitize TRAMP tumorigenesis to ICI treatment. For these studies, we used a sequential combination protocol, where TRAMP mice were treated with Tasquinimod from week 20 through 25, thus coinciding with the peak PMN accumulation in the prostate, followed by administration of anti-PD-1 antibody from weeks 32 to 37 and final harvesting of animal cohorts at 42–45 weeks of age. In these studies, sequential therapy was well tolerated, inhibited TRAMP tumor formation (Fig. 5E), and maintained a prostatic gland architecture, compared to ICI treatment alone (Fig. S6A), with no changes in expression of the neuroendocrine marker, neuron-specific enolase (NSE) (Fig. S6B). Under these conditions, the Tasquinimod+ICI combination abolished the intraprostatic accumulation of $Ly6G^+$ PMN (Fig. S6C) and increased the recruitment of $CD8^+$ T cells (Fig. S6D). This included the expansion of specialized $CD8^+$ T cells that enable therapeutic responses to ICI, including $TCF1^+/PD\text{-}1^+$ (Fig. 5F) and $GrzB^+/KLRG1^+$ (Fig. 5G) subsets, by multiparametric flow cytometry.

DISCUSSION

In this study, we have shown that the NMU neuropeptide, a pleiotropic regulator of cellular homeostasis [29], is overexpressed in primary and metastatic prostate cancer, as well as other malignancies, and enables potent myeloid immunosuppression in the NEPC microenvironment. Mechanistically, NMU reprograms the PMN transcriptome towards an inflammatory and migratory phenotype, suppresses T cell proliferation and maintains tumor growth in vivo. Genetic or pharmacologic targeting of this pathway suppresses NEPC growth, blocks intraprostatic accumulation of PMN and expands specialized $CD8^+$ T cells with 'stem-like', cytotoxic and effector functions, altogether restoring the activity of ICI in this highly refractory malignancy, in vivo (Fig. 5).

Aside from its multiple roles in tissue and organismal homeostasis [31], NMU has emerged as an important regulator of inflammatory responses. This has been linked to recruitment of mast cells [28] and eosinophils [47], protection of gastrointestinal mucosal immunity [27] and stimulation of innate lymphoid cells for production of allergy-related type 2 cytokines [26]. Here, exposure to recombinant NMU was sufficient to extensively remodel the PMN transcriptome, upregulating multiple inflammatory mediators, IFNs and NFκB gene expression [32]. In turn, NMU-stimulated PMN became highly migratory, acquired functional phenotypes of pathologically activated PMN-MDSC [48] and potently inhibited syngeneic T cell proliferation. A role of NMU in regulating an immune tumor microenvironment has been proposed [35] via stimulation of macrophage activation and chemotaxis [49] and release of Th2 cytokines [50]. However, the role of this pathway in T cell responses has remained controversial, linked to inhibition [51] or stimulation [52] of $CD8^+$ T cell antitumor immunity.

One of the key inflammatory mediators upregulated in NMU-stimulated PMN was the DAMP "alarmin", S100A9 [53]. Abundantly expressed by myeloid cells, including PMN-MDSC [54], and released in the extracellular space through various secretory mechanisms [55], S100A9 is a central regulator of the tumor microenvironment. Subverting a physiological role in protection against pathogens [56], S100A9 over-expression in cancer directly accelerates tumor cell proliferation [57], while also driving local immunosuppression via granulocytic MDSC recruitment [58], macrophage polarization [59] and impaired dendritic cell function [60]. In this context, molecules upregulated in NMU-stimulated PMN such as, TREM2 and TNFα are important mediators of S100A9 monocyte polarization [61], and modulation of immature myeloid cells that further contribute to immunosuppression [62]. An NMU/S100A9 signaling axis in immune evasion was established here using complementary transgenic and syngeneic mouse models. However, this pathway may also be at work in the clinic, as bioinformatics analysis of public patient databases highlighted a positive correlation between high NMU levels, reduction of $CD8^+$ T cell, myeloid cell recruitment and immunotherapy resistance with poor outcome.

Among the various models of prostate cancer [63], we tested the relevance of NMU-S100A9 signaling in TRAMP mice [39]. Albeit with known limitations, including the expression of the SV40 foreign antigen that may affect immunogenicity [64], TRAMP mice develop a predominantly AR-independent NEPC phenotype with

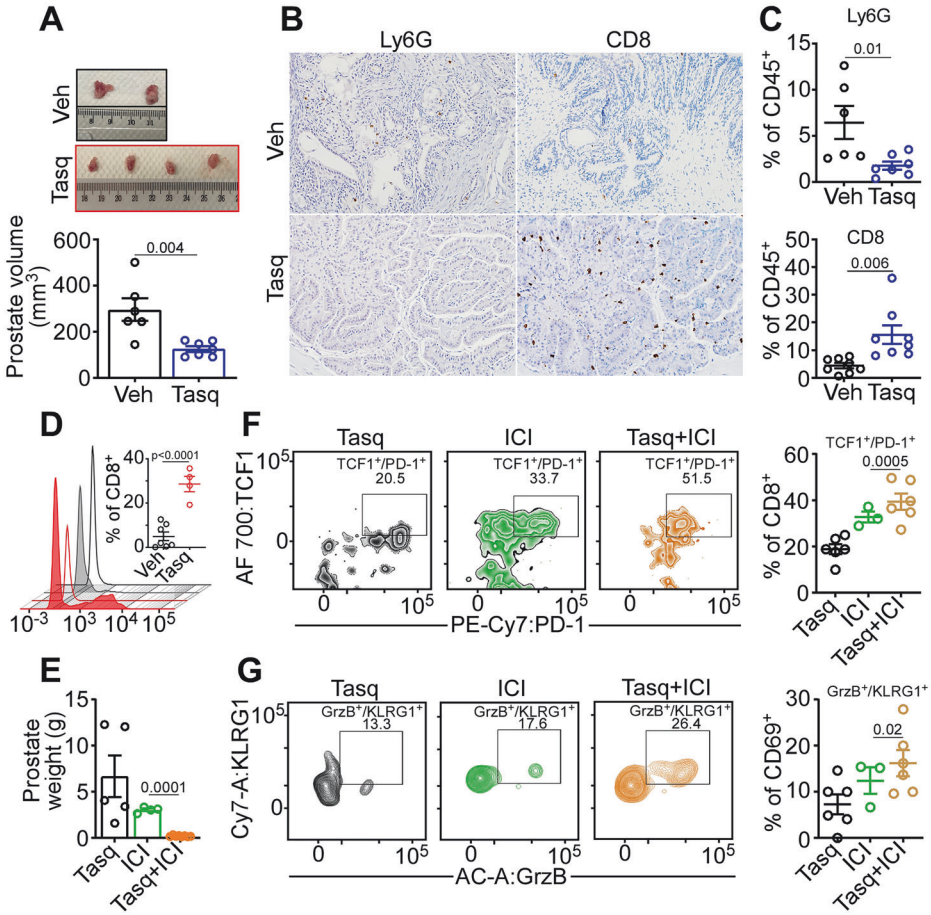


Fig. 5 Preclinical targeting of NMU-S100A9 signaling in NEPC. A TRAMP mice were treated systemically with vehicle (Veh) or S100A9 inhibitor, Tasquinimod (Tasq, 30 mg/kg) starting at week 15 of age for 5 weeks after which treatment was discontinued, and animals were followed until they reached 32 weeks of age for quantification of prostate volume. Mean ± SEM ($n = 6–7$). Inset, representative macroscopic images of prostate tissues from the indicated mouse groups. **B**, **C** The conditions are as in **A** and prostate tissue samples harvested from Veh- or Tasq-treated TRAMP mice at 32 weeks were analyzed by IHC (**B**) and intratumoral accumulation of Ly6G$^+$ PMN (**C**, top) or CD8$^+$ T cells (**C**, bottom) was quantified by multiparametric flow cytometry. Mean ± SEM ($n = 6–7$). **D** The conditions are as in **A** and antigen-specific CD8$^+$ T cells recognized by an SV40 tetramer were detected by multiparametric flow cytometry and quantified (inset). Each symbol is an individual mouse determination. **E** TRAMP mice were sequentially treated with Tasquinimod (15 mg/kg) from week 20 to 25 and then discontinued followed by administration of an antibody to PD-1 (ICI, weeks 32 through 37) and changes in prostate weight were quantified in animals harvested at 42–45 weeks. Animals treated with ICI alone (weeks 32 through 37) were used as control. Mean ± SEM (ICI, $n = 4$; Tasq, $n = 5$; Tasq+ICI, $n = 8$). The conditions are as in (**E**) and prostate tissue samples from TRAMP mice in the various treatment groups were harvested at 42-45 weeks and modulation of TCF1$^+$/PD-1$^+$ (**F**) or GrzB$^+$/KLRG1$^+$ (**G**) CD8$^+$ T cell subsets was detected by multiparametric flow cytometry (left) and quantified (right). The percentage of positive cells is indicated. Representative experiment. Mean ± SEM ($n = 3$-6). For panels **A**, **C**–**G**, numbers are p values by unpaired two-sided t test. Each symbol is an individual mouse determination.

high penetrance and predictable progression. In these settings, intraprostatic NMU as well as S100A9 expression peaked at 17–19 weeks of age, coinciding with the appearance of high-grade PIN [65], recruitment of PMN and depletion of CD8$^+$ T cells. Importantly, these changes were temporally transient, as older TRAMP mice (up to 40 weeks of age) did not exhibit a similar modulation of NMU-S100A9 expression or cellular infiltrate. There is abundant evidence that the cellular composition of a tumor microenvironment is highly dynamic, varying extensively at different stages of tumorigenesis [66]. There is also evidence that early and often transient modulation of an immune, especially myeloid cell infiltrate, profoundly affects later kinetics of tumor growth [67, 68], expression of inflammatory cytokines [69], immune evasion [70] and metastatic dissemination. This is in line with the high levels of NMU that we identified across the spectrum of prostatic tumorigenesis in humans, including AR$^-$/NE$^+$ metastases.

In this context, prostate cancer, especially NEPC, has long been recognized for its immune-excluded microenvironment [71], depleted of CD8$^+$ T cells [72], but saturated with immunosuppressive cues that have hampered, in most trials, the clinical response to ICI [73]. MDSCs play a major role in ICI resistance, driving transition to AR-independence via IL23 secretion [74], inhibiting tumor-specific T cell functions in cooperation with other stromal cells, i.e., mast cells [75], and rewiring arginine metabolism, NO production and redox balance to further promote immune escape [48]. More work is needed to determine if NMU-stimulated PMN acquire the full complement of functional and phenotypic hallmarks of MDSC. MDSC, in addition to their ability to suppress T cell proliferation, NMU-stimulated PMN expressed high levels of CXCR2, which is a central driver of myeloid chemotaxis and treatment resistance in prostate cancer [76], as well as CXCR4, a mediator of prostate cancer bone metastasis [77] and recruitment of immunosuppressive Treg subsets [78].

Against this backdrop, silencing NMU or targeting S100A9 with Tasquinimod [79], potently inhibited NEPC growth in vivo. Mechanistically, this was associated with a reinvigorated anti-tumor immune microenvironment, characterized by reduced PMN

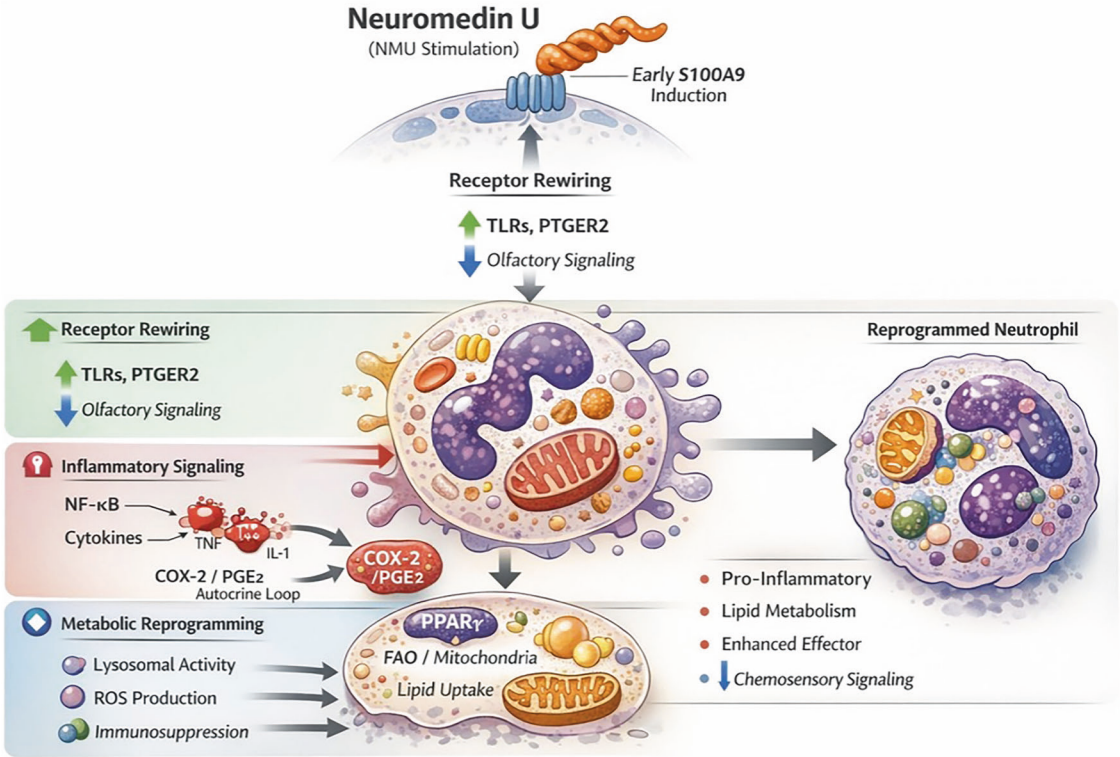


Fig. 6 Schematic diagram of NMU-S100A9 'innervation' in prostate cancer inflammation and immunosuppression.

infiltration and expansion of specialized $CD8^+$ T cell subsets with "stem-like" ($TCF1^+/PD1^+$), effector resident ($CD69^+/KLRG1^+$) and immune killing ($GrzB^+/KLRG1^+$) properties [80, 81]. These T cell subsets are central determinants of the clinical response to immunotherapy [80, 82], and, accordingly, the combination of PD-1 blockade plus NMU silencing or Tasquinimod treatment potently suppressed tumor growth in syngeneic and transgenic (TRAMP) mouse models. Importantly, $CD8^+$ T cells generated in response to NMU-S100A9 targeting were tumor-specific, recognizing the SV40 large T antigen oncogene that drives prostate cancer progression in the TRAMP model [39]. For its immune remodeling properties, Tasquinimod has been intensely investigated in metastatic prostate cancer patients [46], but despite evidence of stable disease [83], no benefits in overall survival were observed in larger trials [84]. The results here provide proof-of-concept evidence to rationally repurpose Tasquinimod in combination with ICI in patients with advanced prostate cancer. This will require carefully optimizing the timing of treatment start, as most patients with ADT/ASRi-associated NEPC are typically diagnosed at advanced disease stages.

In summary, we have shown that NMU signaling is broadly exploited in primary and metastatic prostate cancer, especially NEPC, to confer an inflammatory and immunosuppressive microenvironment that sustains tumor growth in vivo (Fig. 6). This pathway adds a novel pro-tumorigenic circuitry to a growing interface between the neuronal system and the tumor microenvironment, driving immune evasion and disease progression. Conversely, the NMU/S100A9 signaling axis exposes an unprecedented vulnerability in NEPC, potentially suited to reverse immunosuppression [71] and restore sensitivity to ICI in this highly refractory disease variant [85].

DATA AVAILABILITY

The datasets reported in the current study are available from the corresponding author on reasonable request.

REFERENCES

1. Monje M, Borniger JC, D'Silva NJ, Deneen B, Dirks PB, Fattahi F, et al. Roadmap for the emerging field of cancer neuroscience. Cell. 2020;181:219–22.
2. Shi DD, Guo JA, Hoffman HI, Su J, Mino-Kenudson M, Barth JL, et al. Therapeutic avenues for cancer neuroscience: translational frontiers and clinical opportunities. Lancet Oncol. 2022;23:e62–e74.
3. Ayala GE, Dai H, Powell M, Li R, Ding Y, Wheeler TM, et al. Cancer-related axonogenesis and neurogenesis in prostate cancer. Clin Cancer Res. 2008;14:7593–603.
4. Zahalka AH, Arnal-Estape A, Maryanovich M, Nakahara F, Cruz CD, Finley LWS, et al. Adrenergic nerves activate an angio-metabolic switch in prostate cancer. Science. 2017;358:321–6.
5. March B, Faulkner S, Jobling P, Steigler A, Blatt A, Denham J, et al. Tumour innervation and neurosignalling in prostate cancer. Nat Rev Urol. 2020;17:119–30.
6. Magnon C, Hall SJ, Lin J, Xue X, Gerber L, Freedland SJ, et al. Autonomic nerve development contributes to prostate cancer progression. Science. 2013;341:1236361.
7. Di Donato M, Giovannelli P, Migliaccio A, Castoria G. The nerve growth factor-delivered signals in prostate cancer and its associated microenvironment: when the dialogue replaces the monologue. Cell Biosci. 2023;13:60.
8. Kfoury Y, Baryawno N, Severe N, Mei S, Gustafsson K, Hirz T, et al. Human prostate cancer bone metastases have an actionable immunosuppressive microenvironment. Cancer Cell. 2021;39:1464–78.e1468.
9. Brea L, Yu J. Tumor-intrinsic regulators of the immune-cold microenvironment of prostate cancer. Trends Endocrinol Metab. 2025;36:855–66.
10. Coarfa C, Florentin D, Putluri N, Ding Y, Au J, He D, et al. Influence of the neural microenvironment on prostate cancer. Prostate. 2018;78:128–39.
11. Sigorski D, Kasprzyk-Pawelec A, Michalak M, Sosnowski R, Hryciuk MM, Sejda A, et al. The nervous system in prostate cancer: a basic science and clinical perspective. Semin Oncol. 2026;53:152425.
12. Aggarwal R, Huang J, Alumkal JJ, Zhang L, Feng FY, Thomas GV, et al. Clinical and genomic characterization of treatment-emergent small-cell neuroendocrine prostate cancer: a multi-institutional prospective study. J Clin Oncol. 2018;36:2492–503.
13. Bluemn EG, Coleman IM, Lucas JM, Coleman RT, Hernandez-Lopez S, Tharakan R, et al. Androgen receptor pathway-independent prostate cancer is sustained through FGF signaling. Cancer Cell. 2017;32:474–89.e476.
14. Ryan CJ, Smith MR, Fizazi K, Saad F, Mulders PF, Sternberg CN, et al. Abiraterone acetate plus prednisone versus placebo plus prednisone in chemotherapy-naive men with metastatic castration-resistant prostate cancer (COU-AA-302): final

overall survival analysis of a randomised, double-blind, placebo-controlled phase 3 study. Lancet Oncol. 2015;16:152–60.
15. Zou M, Toivanen R, Mitrofanova A, Floch N, Hayati S, Sun Y, et al. Transdifferentiation as a mechanism of treatment resistance in a mouse model of castration-resistant prostate cancer. Cancer Discov. 2017;7:736–49.
16. Dardenne E, Beltran H, Benelli M, Gayvert K, Berger A, Puca L, et al. N-Myc induces an EZH2-mediated transcriptional program driving neuroendocrine prostate cancer. Cancer Cell. 2016;30:563–77.
17. Lee JK, Phillips JW, Smith BA, Park JW, Stoyanova T, McCaffrey EF, et al. N-Myc drives neuroendocrine prostate cancer initiated from human prostate epithelial cells. Cancer Cell. 2016;29:536–47.
18. Park JW, Lee JK, Sheu KM, Wang L, Balanis NG, Nguyen K, et al. Reprogramming normal human epithelial tissues to a common, lethal neuroendocrine cancer lineage. Science. 2018;362:91–95.
19. Li Q, Deng Q, Chao HP, Liu X, Lu Y, Lin K, et al. Linking prostate cancer cell AR heterogeneity to distinct castration and enzalutamide responses. Nat Commun. 2018;9:3600.
20. Wang HT, Yao YH, Li BG, Tang Y, Chang JW, Zhang J. Neuroendocrine Prostate Cancer (NEPC) progressing from conventional prostatic adenocarcinoma: factors associated with time to development of NEPC and survival from NEPC diagnosis-a systematic review and pooled analysis. J Clin Oncol. 2014;32:3383–90.
21. Vanden Abeele F, Salzet M. The neuro-immune oncology axis. Cancer Lett. 2025;634:218070.
22. Liu Z, Peng Q, Wang Y, Chiu PK, Teoh JY, Wang R, et al. Neuroscience in prostate cancer. Prostate Cancer Prostatic Dis. 2026;29:478–87.
23. Venkatesh HS, Tam LT, Woo PJ, Lennon J, Nagaraja S, Gillespie SM, et al. Targeting neuronal activity-regulated neuroligin-3 dependency in high-grade glioma. Nature. 2017;549:533–7.
24. Aysit N, Altintas E, Koksalar Alkan F, Ozturk G, Korkaya H. The neural niche in cancer: mechanistic insights into tumor-neuron-immune crosstalk and therapeutic opportunities. Front Cell Dev Biol. 2026;14:1667459.
25. Gandhi S, Pandey MR, Attwood K, Ji W, Witkiewicz AK, Knudsen ES, et al. Phase I clinical trial of combination propranolol and pembrolizumab in locally advanced and metastatic melanoma: safety, tolerability, and preliminary evidence of antitumor activity. Clin Cancer Res. 2021;27:87–95.
26. Klose CSN, Mahlakoiv T, Moeller JB, Rankin LC, Flamar AL, Kabata H, et al. The neuropeptide neuromedin U stimulates innate lymphoid cells and type 2 inflammation. Nature. 2017;549:282–6.
27. Li Y, Liu S, Zhou K, Wang Y, Chen Y, Hu W, et al. Neuromedin U programs eosinophils to promote mucosal immunity of the small intestine. Science. 2023;381:1189–96.
28. Moriyama M, Sato T, Inoue H, Fukuyama S, Teranishi H, Kangawa K, et al. The neuropeptide neuromedin U promotes inflammation by direct activation of mast cells. J Exp Med. 2005;202:217–24.
29. Martinez VG, O'Driscoll L. Neuromedin U: a multifunctional neuropeptide with pleiotropic roles. Clin Chem. 2015;61:471–82.
30. Dcunha L, Edakkad B, Fathima I, Dagamajalu S, Raju R, Devasahayam Arokia Balaya R, et al. Neuromedin U signaling map: toward neuropeptide focused therapeutic targets in cancer and human diseases. OMICS. 2026;30:211–23.
31. Malendowicz LK, Rucinski M. Neuromedins NMU and NMS: an updated overview of their functions. Front Endocrinol. 2021;12:713961.
32. Raddatz R, Wilson AE, Artymyshyn R, Bonini JA, Borowsky B, Boteju LW, et al. Identification and characterization of two neuromedin U receptors differentially expressed in peripheral tissues and the central nervous system. J Biol Chem. 2000;275:32452–9.
33. Przygodzka P, Soboska K, Sochacka E, Boncela J. Neuromedin U: a small peptide in the big world of cancer. Cancers. 2019;11:1312.
34. Benzaquen D, Lawrence YR, Taussky D, Zwahlen D, Oehler C, Champion A. The crosstalk between nerves and cancer-A poorly understood phenomenon and new possibilities. Cancers. 2024;16:1875.
35. Przygodzka P, Szulc-Kielbik I, Kielbik M, Pacholczyk M, Klink M. Neuromedin U in the tumor microenvironment - Possible actions in tumor progression. Biochim Biophys Acta Rev Cancer. 2025;1880:189269.
36. Dobin A, Davis CA, Schlesinger F, Drenkow J, Zaleski C, Jha S, et al. STAR: ultrafast universal RNA-seq aligner. Bioinformatics. 2013;29:15–21.
37. Li B, Dewey CN. RSEM: accurate transcript quantification from RNA-Seq data with or without a reference genome. BMC Bioinforma. 2011;12:323.
38. Love MI, Huber W, Anders S. Moderated estimation of fold change and dispersion for RNA-seq data with DESeq2. Genome Biol. 2014;15:550.
39. Berman-Booty LD, Sargeant AM, Rosol TJ, Rengel RC, Clinton SK, Chen CS, et al. A review of the existing grading schemes and a proposal for a modified grading scheme for prostatic lesions in TRAMP mice. Toxicol Pathol. 2012;40:5–17.
40. Zaidi S, Park J, Chan JM, Roudier MP, Zhao JL, Gopalan A, et al. Single cell analysis of treatment-resistant prostate cancer: implications of cell state changes for cell surface antigen targeted therapies. Proc Natl Acad Sci USA. 2024;121:e2322203121.
41. Labrecque MP, Coleman IM, Brown LG, True LD, Kollath L, Lakely B, et al. Molecular profiling stratifies diverse phenotypes of treatment-refractory metastatic castration-resistant prostate cancer. J Clin Invest. 2019;129:4492–505.
42. Zheng Q, Xie X, Guo Q, Chen C, Jiang W. Prognostic value of tumor-infiltrating lymphocytes and common subtypes in patients with gastroenteropancreatic neuroendocrine neoplasms: a systematic review and meta-analysis. BMC Cancer. 2026;26:793.
43. Yeung AML, Chow JCH. Management of pulmonary large-cell neuroendocrine carcinoma (LCNEC): an updated review. Clin Lung Cancer. 2026;27:85–97.
44. Chen D, Ayala GE. Innervating prostate cancer. N Engl J Med. 2018;378:675–7.
45. Dysthe M, Parihar R. Myeloid-derived suppressor cells in the tumor microenvironment. Adv Exp Med Biol. 2020;1224:117–40.
46. Brower V. Tasquinimod treatment for prostate cancer. Lancet Oncol. 2016;17:e322.
47. Moriyama M, Fukuyama S, Inoue H, Matsumoto T, Sato T, Tanaka K, et al. The neuropeptide neuromedin U activates eosinophils and is involved in allergen-induced eosinophilia. Am J Physiol Lung Cell Mol Physiol. 2006;290:L971–977.
48. Gabrilovich DI, Nagaraj S. Myeloid-derived suppressor cells as regulators of the immune system. Nat Rev Immunol. 2009;9:162–74.
49. Przygodzka P, Soboska K, Sochacka E, Pacholczyk M, Braun M, Kassassir H, et al. Neuromedin U secreted by colorectal cancer cells promotes a tumour-supporting microenvironment. Cell Commun Signal. 2022;20:193.
50. Johnson EN, Appelbaum ER, Carpenter DC, Cox RF, Disa J, Foley JJ, et al. Neuromedin U elicits cytokine release in murine Th2-type T cell clone D10.G4.1. J Immunol. 2004;173:7230–8.
51. Zheng R, Wang S, Wang J, Zhou M, Shi Q, Liu B. Neuromedin U regulates the antitumor activity of CD8(+) T cells and glycolysis of tumor cells in the tumor microenvironment of pancreatic ductal adenocarcinoma in an NMUR1-dependent manner. Cancer Sci. 2024;115:334–46.
52. Zhou Y, Zhang X, Gao Y, Peng Y, Liu P, Chen Y, et al. Neuromedin U receptor 1 deletion leads to impaired immunotherapy response and high malignancy in colorectal cancer. iScience. 2024;27:110318.
53. Chen Y, Ouyang Y, Li Z, Wang X, Ma J. S100A8 and S100A9 in cancer. Biochim Biophys Acta Rev Cancer. 2023;1878:188891.
54. Eisenblaetter M, Flores-Borja F, Lee JJ, Wefers C, Smith H, Hueting R, et al. Visualization of tumor-immune interaction - target-specific imaging of S100A8/A9 reveals pre-metastatic niche establishment. Theranostics. 2017;7:2392–401.
55. Sprenkeler EGG, Zandstra J, van Kleef ND, Goetschalckx I, Verstegen B, Aarts CEM, et al. S100A8/A9 is a marker for the release of neutrophil extracellular traps and induces neutrophil activation. Cells. 2022;11:236.
56. Silvin A, Chapuis N, Dunsmore G, Goubet AG, Dubuisson A, Derosa L, et al. Elevated calprotectin and abnormal myeloid cell subsets discriminate severe from mild COVID-19. Cell. 2020;182:1401–18.e1418.
57. Wu R, Duan L, Cui F, Cao J, Xiang Y, Tang Y, et al. S100A9 promotes human hepatocellular carcinoma cell growth and invasion through RAGE-mediated ERK1/2 and p38 MAPK pathways. Exp Cell Res. 2015;334:228–38.
58. Yang Q, Li X, Chen H, Cao Y, Xiao Q, He Y, et al. IRF7 regulates the development of granulocytic myeloid-derived suppressor cells through S100A9 transrepression in cancer. Oncogene. 2017;36:2969–80.
59. Kwak T, Wang F, Deng H, Condamine T, Kumar V, Perego M, et al. Distinct populations of immune-suppressive macrophages differentiate from monocytic myeloid-derived suppressor cells in cancer. Cell Rep. 2020;33:108571.
60. Maus RLG, Jakub JW, Nevala WK, Christensen TA, Noble-Orcutt K, Sachs Z, et al. Human melanoma-derived extracellular vesicles regulate dendritic cell maturation. Front Immunol. 2017;8:358.
61. Zhou L, Wang M, Guo H, Hou J, Zhang Y, Li M, et al. Integrated analysis highlights the immunosuppressive role of TREM2(+) macrophages in hepatocellular carcinoma. Front Immunol. 2022;13:848367.
62. Sade-Feldman M, Kanterman J, Ish-Shalom E, Elnekave M, Horwitz E, Baniyash M. Tumor necrosis factor-alpha blocks differentiation and enhances suppressive activity of immature myeloid cells during chronic inflammation. Immunity. 2013;38:541–54.
63. Ittmann M, Huang J, Radaelli E, Martin P, Signoretti S, Sullivan R, et al. Animal models of human prostate cancer: the consensus report of the New York meeting of the Mouse Models of Human Cancers Consortium Prostate Pathology Committee. Cancer Res. 2013;73:2718–36.
64. Hensley PJ, Kyprianou N. Modeling prostate cancer in mice: limitations and opportunities. J Androl. 2012;33:133–44.
65. Irshad S, Abate-Shen C. Modeling prostate cancer in mice: something old, something new, something premalignant, something metastatic. Cancer Metastasis Rev. 2013;32:109–22.
66. de Visser KE, Joyce JA. The evolving tumor microenvironment: from cancer initiation to metastatic outgrowth. Cancer Cell. 2023;41:374–403.

67. Chia K, Mazzolini J, Mione M, Sieger D. Tumor initiating cells induce Cxcr4-mediated infiltration of pro-tumoral macrophages into the brain. Elife. 2018;7:e31918.
68. Linde N, Casanova-Acebes M, Sosa MS, Mortha A, Rahman A, Farias E, et al. Macrophages orchestrate breast cancer early dissemination and metastasis. Nat Commun. 2018;9:21.
69. Asano K, Takahashi N, Ushiki M, Monya M, Aihara F, Kuboki E, et al. Intestinal CD169(+) macrophages initiate mucosal inflammation by secreting CCL8 that recruits inflammatory monocytes. Nat Commun. 2015;6:7802.
70. Schlesinger Y, Yosefov-Levi O, Kolodkin-Gal D, Granit RZ, Peters L, Kalifa R, et al. Single-cell transcriptomes of pancreatic preinvasive lesions and cancer reveal acinar metaplastic cells' heterogeneity. Nat Commun. 2020;11:4516.
71. Bhinder B, Ferguson A, Sigouros M, Uppal M, Elsaeed AG, Bareja R, et al. Immunogenomic landscape of neuroendocrine prostate cancer. Clin Cancer Res. 2023;29:2933–43.
72. Romero R, Chu T, Gonzalez Robles TJ, Smith P, Xie Y, Kaur H, et al. The neuroendocrine transition in prostate cancer is dynamic and dependent on ASCL1. Nat Cancer. 2024;5:1641–59.
73. Goswami S, Aparicio A, Subudhi SK. Immune checkpoint therapies in prostate cancer. Cancer J. 2016;22:117–20.
74. Calcinotto A, Spataro C, Zagato E, Di Mitri D, Gil V, Crespo M, et al. IL-23 secreted by myeloid cells drives castration-resistant prostate cancer. Nature. 2018; 559:363–9.
75. Jachetti E, Cancila V, Rigoni A, Bongiovanni L, Cappetti B, Belmonte B, et al. Cross-talk between myeloid-derived suppressor cells and mast cells mediates tumor-specific immunosuppression in prostate cancer. Cancer Immunol Res. 2018;6:552–65.
76. Guo C, Sharp A, Gurel B, Crespo M, Figueiredo I, Jain S, et al. Targeting myeloid chemotaxis to reverse prostate cancer therapy resistance. Nature. 2023;623:1053–61.
77. Taichman RS, Cooper C, Keller ET, Pienta KJ, Taichman NS, McCauley LK. Use of the stromal cell-derived factor-1/CXCR4 pathway in prostate cancer metastasis to bone. Cancer Res. 2002;62:1832–7.
78. Li J, Zhang L, Liu R, Xu C, Tang H, Zou Y, et al. CXCL12/CXCR4 axis governs Treg spatial dominance over CD8+ T cells via IL-2 sequestration: a dual therapeutic target in prostate cancer. Front Immunol. 2025;16:1626708.
79. Raymond E, Dalgleish A, Damber JE, Smith M, Pili R. Mechanisms of action of tasquinimod on the tumour microenvironment. Cancer Chemother Pharm. 2014;73:1–8.
80. Siddiqui I, Schaeuble K, Chennupati V, Fuertes Marraco SA, Calderon-Copete S, Pais Ferreira D, et al. Intratumoral Tcf1(+)PD-1(+)CD8(+) T cells with stem-like properties promote tumor control in response to vaccination and checkpoint blockade immunotherapy. Immunity. 2019;50:195–211.e110.
81. Cullen SP, Brunet M, Martin SJ. Granzymes in cancer and immunity. Cell Death Differ. 2010;17:616–23.
82. Miller BC, Sen DR, Al Abosy R, Bi K, Virkud YV, LaFleur MW, et al. Subsets of exhausted CD8(+) T cells differentially mediate tumor control and respond to checkpoint blockade. Nat Immunol. 2019;20:326–36.
83. Pili R, Haggman M, Stadler WM, Gingrich JR, Assikis VJ, Bjork A, et al. Phase II randomized, double-blind, placebo-controlled study of tasquinimod in men with minimally symptomatic metastatic castrate-resistant prostate cancer. J Clin Oncol. 2011;29:4022–8.
84. Sternberg C, Armstrong A, Pili R, Ng S, Huddart R, Agarwal N, et al. Randomized, double-blind, placebo-controlled phase III study of tasquinimod in men with metastatic castration-resistant prostate cancer. J Clin Oncol. 2016;34:2636–43.
85. Lyu A, Fan Z, Clark M, Lea A, Luong D, Setayesh A, et al. Evolution of myeloid-mediated immunotherapy resistance in prostate cancer. Nature. 2025;637:1207–17.

ACKNOWLEDGEMENTS

We thank Dr. Marcus Ruscetti (UMASS Chan Medical School) for mouse prostate cancer cell lines MPten-1 and MP3098. We thank Wistar Histotechnology, Imaging and Genomics Facility for the technical support. We thank NIH Tetramer Core Facility at Emory for providing SV40 and Ctrl Tetramers.

AUTHOR CONTRIBUTIONS

Conceptualization: MP, DCA; Methodology: MP, FCA, JM, AVK, MT, MMT, FL, CL, GG, JJ; Investigation: MP; FCA, MT, FL, MVI; Visualization: MP, DCA, MT, JJ; Funding acquisition: DCA; Project administration: MP, FCA, AF, DWG, NJP, DG, LRL, DCA; Supervision: MP, NJP, DCA; Writing – original draft: MP, DCA.

FUNDING

This work was supported by NIH R01 grant CA234162 (DWG) and the Prostate Cancer Foundation with award 22CHAL13 (DWG).

COMPETING INTERESTS

The authors declare no competing interests.

ADDITIONAL INFORMATION

Supplementary information The online version contains supplementary material available at https://doi.org/10.1038/s41388-026-03969-5.

Correspondence and requests for materials should be addressed to Michela Perego.

Reprints and permission information is available at http://www.nature.com/reprints

Publisher's note Springer Nature remains neutral with regard to jurisdictional claims in published maps and institutional affiliations.

Springer Nature or its licensor (e.g. a society or other partner) holds exclusive rights to this article under a publishing agreement with the author(s) or other rightsholder(s); author self-archiving of the accepted manuscript version of this article is solely governed by the terms of such publishing agreement and applicable law.